Author/s:
Zhao, C;Feng, F;Hou, J;Hu, J;Su, Y;Liu, JZ;Hill, M;Freeman, BD;Wang, H;Zhang, H

Title:
Unlocking Direct Lithium Extraction in Harsh Conditions through Thiol-Functionalized Metal-Organic Framework Subnanofluidic Membranes

Date:
2024-05-22

Citation:
Zhao, C., Feng, F., Hou, J., Hu, J., Su, Y., Liu, J. Z., Hill, M., Freeman, B. D., Wang, H. & Zhang, H. (2024). Unlocking Direct Lithium Extraction in Harsh Conditions through Thiol-Functionalized Metal-Organic Framework Subnanofluidic Membranes. Journal of the American Chemical Society, 146 (20), pp.14058-14066. https://doi.org/10.1021/jacs.4c02477.

JACS
JOURNAL OF THE AMERICAN CHEMICAL SOCIETY
pubs.acs.org/JACS
Article

Unlocking Direct Lithium Extraction in Harsh Conditions through Thiol-Functionalized Metal−Organic Framework Subnanofluidic Membranes

Chen Zhao,[#] Fan Feng,[#] Jue Hou,[*] Jian Hu, Yuyu Su, Jefferson Zhe Liu,[*] Matthew Hill, Benny D. Freeman, Huanting Wang, and Huacheng Zhang[*]

Cite This: J. Am. Chem. Soc. 2024, 146, 14058−14066
Read Online

ACCESS | Metrics & More | Article Recommendations | Supporting Information

ABSTRACT: Metal−organic framework (MOF) membranes with high ion selectivity are highly desirable for direct lithium-ion (Li^+) separation from industrial brines. However, very few MOF membranes can efficiently separate Li^+ from brines of high Mg^{2+}/Li^+ concentration ratios and keep stable in ultrahigh Mg^{2+}-concentrated brines. This work reports a type of MOF-channel membranes (MOFCMs) by growing UiO-66-$(SH)_2$ into the nanochannels of polymer substrates to improve the efficiency of MOF membranes for challenging Li^+ extraction. The resulting membranes demonstrate excellent monovalent metal ion selectivity over divalent metal ions, with Li^+/Mg^{2+} selectivity up to 10^3 since Mg^{2+} should overcome a higher energy barrier than Li^+ when transported through the MOF pores, as confirmed by molecular dynamics simulations. Under dual-ion diffusion, as the Mg^{2+}/Li^+ mole ratio of the feed solution increases from 0.2 to 30, the membrane Li^+/Mg^{2+} selectivity decreases from 1516 to 19, corresponding to the purity of lithium products between 99.9 and 95.0%. Further research on multi-ion diffusion that involves Mg^{2+} and three monovalent metal ions (K^+, Na^+, and Li^+, referred to as M^+) in the feed solutions shows a significant improvement in Li^+/Mg^{2+} separation efficiency. The Li^+/Mg^{2+} selectivity can go up to 1114 when the Mg^{2+}/M^+ molar concentration ratio is 1:1, and it remains at 19 when the ratio is 30:1. The membrane selectivity is also stable for 30 days in a highly concentrated solution with a high Mg^{2+}/Li^+ concentration ratio. These results indicate the feasibility of the MOFCMs for direct lithium extraction from brines with Mg^{2+} concentrations up to 3.5 M. This study provides an alternative strategy for designing efficient MOF membranes in extracting valuable minerals in the future.

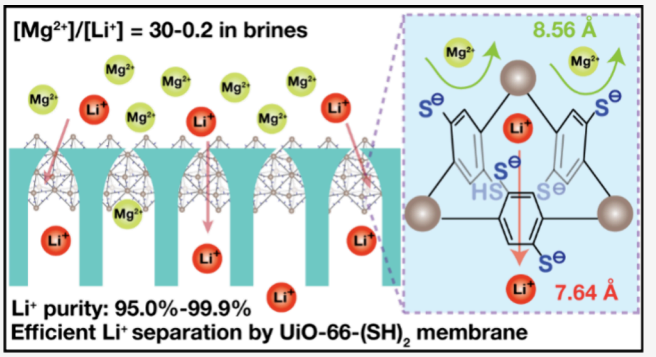

INTRODUCTION

Ion-selective nanofluidic membranes are excellent candidates for extracting and recovering valuable lithium ions (Li^+) from salt-lake brines and other Li^+-rich resources.[1,2] Recent developments in membranes with pore sizes <1 nm have attracted intensive research interest due to their enhanced ion sieving properties.[3−8] Among the available options, angstrom-porous metal−organic framework (MOF) membranes have emerged as competitive candidates for ion separation due to their well-defined pore sizes and tunable pore structures and chemistries,[9−15] especially for addressing Li^+/Mg^{2+} separation during lithium extraction processes. Polycrystalline MOF thin film membranes (MOFTFMs), consisting of an intergrown MOF (e.g., UiO-66,[16] UiO-66-NH_2,[17] UiO-66-$(COONa)_2$,[18] UiO-66-$(COOH)_2$/UiO-66-NH_2,[19] UiO-67,[20] ZIF-8,[21] HKUST-1[22]) crystal layer or deposited/cross-linked MOF (e.g., ZIF-7,[23] UiO-66-NH_2[24]) particles directly covering the top surface of nanoporous substrates, have shown impressive separation performance with high Li^+/Mg^{2+} selectivity ranging between 10^1 and 10^3. As only a few MOFs could be synthesized into defect-free MOFTFMs, MOF-based mixed matrix membranes (MOFMMMs) and MOF-channel membranes (MOFCMs) that allow a wide selection of MOFs for membrane fabrication have emerged as alternative candidates for ion separation. MOFMMMs were composed of MOF particles (e.g., UiO-66,[25] UiO-66-SO_3H,[25,26] MOF-808,[25] ZIF-8,[25] and Zn-TCPP[27]) as fillers and polymers as matrixes, while MOFCMs were fabricated by growing MOF crystals (e.g., UiO-66-$(COOH)_2$[28] and HKUST-1[29]) inside the nanochannels of membrane substrates. Because of the existence of defects between MOFs and substrates, Li^+/Mg^{2+} selectivity of these MOFMMMs and MOFCMs were between 5 and 50,

Received: February 19, 2024
Revised: April 30, 2024
Accepted: May 1, 2024
Published: May 11, 2024

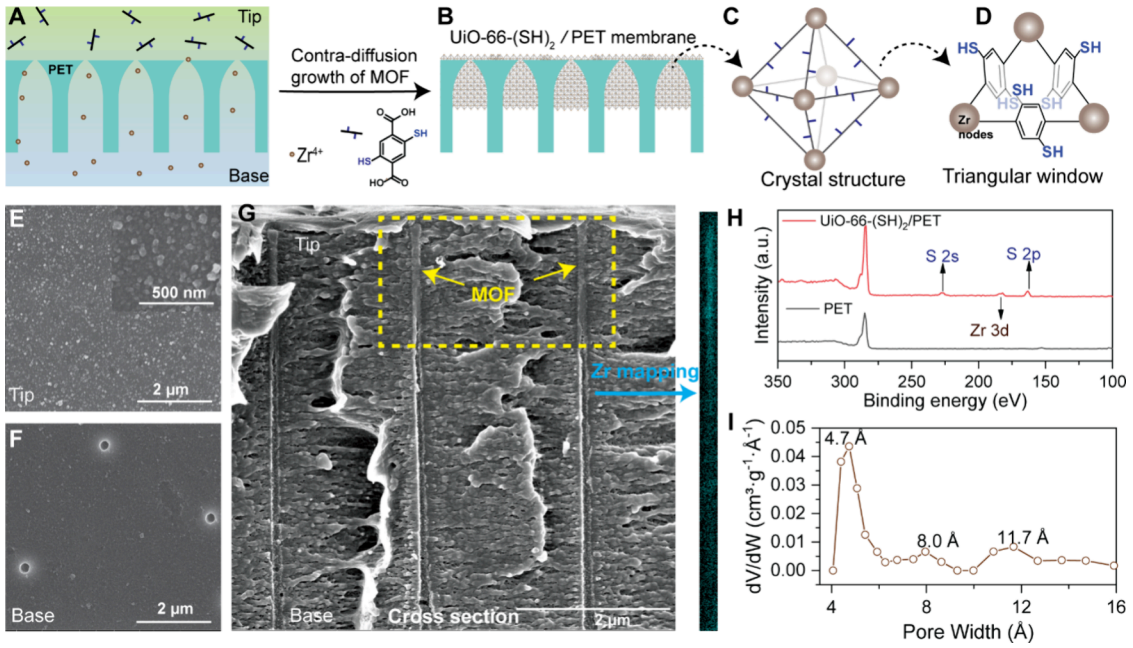

Figure 1. Fabrication and characterizations of the UiO-66-$(SH)_2$/PET membrane. (A, B) Contra-diffusion growth of MOF crystals within the PET membrane. (C, D) Schematics of the UiO-66-$(SH)_2$ MOF unit cell and triangular window structure. (E–G) SEM images of the membrane tip side, base side, and cross section with Zr mapping. (H) XPS survey patterns of the membrane. (I) Pore size distribution of the UiO-66-$(SH)_2$ particles.

which was one to two orders of magnitude less than that of their single-channel devices[28] and MOFTFMs.[21,22] Therefore, it is of great significance to explore new MOFs for synthesizing high-quality, MOF-based membranes for efficient ion separation.

Most current membranes for the Li^+/Mg^{2+} separation have been evaluated under conditions with equal concentrations of Li^+ and Mg^{2+} in dual-ion separation experiments, which is used as a facile and straightforward standard for evaluating the ion separation performance and mechanism of different membranes. Since the concentration ratio between Mg^{2+} and Li^+ in global salt-lake brines is variable between 10^{-1} and 10^2,[30,31] and some brines are of high ion salinity with Mg^{2+} concentrations up to 3 M,[31] membrane-based Li^+/Mg^{2+} separation is more challenging and demands a more comprehensive evaluation regarding the ion species concentration and composition. To effectively address this critical challenge, MOF membranes must be durable and stable enough to block concentrated Mg^{2+} ions while still allowing for the transport of limited Li^+ ions. To further improve the Li^+/Mg^{2+} selectivity of UiO-66 MOFCMs for real applications, one strategy is to manipulate the surface chemistry of the MOF crystals to increase the divalent ion blockage capability. Thiol-functionalized UiO-66 MOF, UiO-66-$(SH)_2$, with angstrom-scale pore sizes and strong binding capability to divalent metal ions, such as Hg^{2+} and Pb^{2+} in wastewater,[32,33] would be an excellent platform to fabricate a lithium-selective membrane.

Herein, UiO-66-$(SH)_2$ MOFCMs are fabricated using a contra-diffusion method. The cation transport properties (K^+, Na^+, Li^+, Ca^{2+}, and Mg^{2+}) of the membranes were first investigated in single-electrolyte solutions with different ion concentrations and pH values. The membrane shows excellent ideal K^+/Mg^{2+} and Li^+/Mg^{2+} selectivities of 2241 and 447, respectively, at 0.1 M and pH 6. Additionally, in the dual-ion permeation experiments with different synthetic brines, the membrane Li^+/Mg^{2+} selectivity increases from 19 to 1516 as the Mg^{2+}/Li^+ mole ratios in brine decrease from 30 to 0.2. Also, in the multi-ion diffusion system containing Mg^{2+} and three monovalent metal ions (i.e., K^+, Na^+, and Li^+, noted by M^+) in the feed solutions, the Li^+/Mg^{2+} selectivity reaches 1114 at a Mg^{2+}/M^+ molar concentration ratio of 1:1 and maintains 19 at a Mg^{2+}/M^+ mole ratio of 30:1. Thus, the membranes possess a decent capability for Li^+/Mg^{2+} separation from brines with high Mg^{2+} concentrations and Mg^{2+}/Li^+ concentration ratios. Molecular dynamics (MD) simulations were also performed to elucidate the ion sieving mechanisms in UiO-66-$(SH)_2$. This study opens an alternative avenue to develop MOF membranes for efficient lithium recovery.

RESULTS AND DISCUSSION

Fabrication of the UiO-66-$(SH)_2$ Membrane. The bullet-shaped polyethylene terephthalate (PET) multichannel membrane was prepared by chemical etching of the ion-tracked PET films with a certain pore density (e.g., 10^6 channels cm^{-2}).[34] This resulted in a PET substrate with small pores (29.7 ± 6.0 nm) at the tip side and large pores (192 ± 23.2 nm) at the base side (Figure S1A,B). To investigate the effect of the substrate's pore structure, growth method, and functional groups on ion separation property, UiO-66-$(SH)_2$ membranes were also fabricated by adopting a cylindrical PET substrate or in situ growth method; UiO-66 membranes and amine- and sulfonic-group-modified (UiO-66-NH_2 and UiO-66-SO_3H) membranes were also fabricated. As illustrated in Figure 1A, the UiO-66-$(SH)_2$ membranes were fabricated by contra-diffusion of zirconium ions (Zr^{4+}) and 2,5-dimercaptoterephthalic acid (BDC-$(SH)_2$) through the etched PET substrate by solvothermal reaction. This contra-diffusion method targets an asymmetric growth of the MOF particles mainly near the tip side of the membrane (Figure 1B). Figure 1C,D exhibits the enlarged MOF cell unit structure and window structure that are anchored with double –SH groups. The surfaces (tip and base sides) and cross-sectional

https://doi.org/10.1021/jacs.4c02477
J. Am. Chem. Soc. 2024, 146, 14058–14066

morphology of the UiO-66-$(SH)_2$ membranes were characterized by scanning electron microscopy (SEM). Compared with the smooth surfaces and channels of bare PET membranes (Figure S1C−E), MOF particles are mainly observed at the tip side rather than the base side of the MOF membrane (Figure 1E,F) and the channel areas near the tip side (Figure 1G, indicated by yellow dashed rectangles). Elemental mapping by energy-dispersive X-ray spectroscopy (EDS) on the cross section of the membrane confirms the growth of the MOF within PET nanochannels and the preferential distribution of the MOF near the tip side of the membrane (Figure 1G and Figure S2). Elemental characterization to the membrane tip side by X-ray photoelectron spectroscopy (XPS) detects the elements of zirconium (Zr 3d) at 182.6 eV and sulfur (S 2s and S 2p) at 227.7 and 163.3 eV (Figure 1H) and the Zr−O coordination at 530.6 eV by high-resolution XPS analysis (Figure S3). UiO-66-$(SH)_2$ powders were prepared for characterizing the MOF crystals formed in the membranes, including powder X-ray diffraction (PXRD), SEM, Fourier transform infrared spectroscopy (FTIR), and gas adsorption/desorption. The crystalline structure of MOF particles grown on the membrane tip side was verified by PXRD. They demonstrate the same characteristic peaks as the synthesized UiO-66-$(SH)_2$ powder sample (Figure S4A, B). The synthesized MOF powders are round particles (Figure S4C) that are like the ones formed on the surface of the MOF membrane tip side (Figure S4D). They show a characteristic peak of thiol groups at 2550 cm^{-1} in the FTIR spectrum (Figure S4E) and possess a specific surface area of 276.5 m^2/g (Figure S4F) as well as a 3D pore size distribution in the UiO-66-$(SH)_2$ cell unit: a small window size of ∼4.7 Å and two cavity sizes of about 8 and 11.7 Å, respectively (Figure 1I), which are consistent with a literature report.[33]

Basic Ion Transport Properties. To investigate the ion transport property of the UiO-66-$(SH)_2$ membrane, ion current−voltage (I−V) curves were measured from −1 to +1 V using 0.1 M metal chloride solutions. The I−V curves (Figure 2A) reveal that the membrane exhibits an ion current rectification (ICR) property, resulting from the enhanced charge density provided by MOF crystals at the tip side of the membrane. The ion current values also demonstrate that the membrane transports monovalent cations (K^+, Na^+, and Li^+) much faster than divalent cations (Mg^{2+}, Ca^{2+}). The membrane's mono/divalent ion selectivity for K^+/Mg^{2+}, Na^+/Mg^{2+}, and Li^+/Mg^{2+} could reach 2241, 1215, and 477, respectively (Figure 2B). Further increasing the testing voltage (e.g., 2−4 V) will increase the ion conductance but will also enhance Mg^{2+} transport and ultimately decrease the ion selectivity (Figure S5).

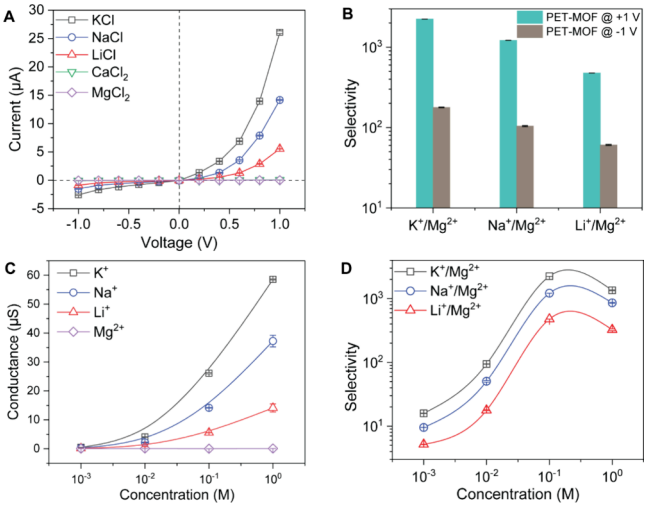

Figure 2. Ion transport, conductance, and selectivity performance of the UiO-66-$(SH)_2$ membrane at (A, B) 0.1 M salt solutions and (C, D) varying concentrations of salt solutions.

The selective ion transport properties can be explained by two aspects. First, the pores of UiO-66-$(SH)_2$ (4.7 Å) are smaller than the diameters of hydrated ions[35] (Table S1), so the ions must overcome the energy barriers to pass through the MOF pores. A detailed discussion of this aspect is provided in MD simulation section. Second, according to our previous studies of MOF subnanofluidic channels,[36−38] the interactions between MOF functional groups and ions, such as binding due to the electrostatic interaction, can regulate the selectivity of ion transport. To investigate the interactions of ions with −SH groups in this work, the surface charge of UiO-66-$(SH)_2$ particles was analyzed by measuring their zeta potentials. This MOF carries a highly negative charge in water (−75 mV) due to deprotonation of the −SH groups, while the surface charges of the MOF particles decrease when dispersed in salt solutions (Table S2). Notably, the reduction is more significant for divalent cations (e.g., dropping to −9.5 mV for Mg^{2+} and reversing to +3.9 mV for Ca^{2+}) than for monovalent cations (e.g., −57 mV for K^+, −59 mV for Na^+, and −61 mV for Li^+). This indicates that −SH groups in the MOF exhibit a stronger binding capability with divalent cations than monovalent cations. To confirm these different binding interactions, XPS analysis of MOF particles dispersed in different salt solutions was conducted and the atomic ratios of cations bound to the MOF were calculated. As shown in Table S3, the divalent cations display a higher percentage value (∼1.8% for Mg^{2+} and ∼2.1% for Ca^{2+}) than that of the monovalent cations (∼0.6% for K^+ and Na^+) in MOF particles, consistent with the stronger binding results of −SH groups with divalent cations.

The ion transport and separation performance of other forms of UiO-66-$(SH)_2$ membranes, i.e., cylindrical PET-UiO-66-$(SH)_2$ and in situ growth UiO-66-$(SH)_2$, were also investigated (Figure S6). Both membranes could not achieve comparable high selectivity (Li^+/Mg^{2+} selectivity <20) and the ion current values drop a lot, because both methods tend to grow MOF crystals in the whole PET channels and block the transport of monovalent cations.

The UiO-66, UiO-66-NH_2, and UiO-66-SO_3H membranes prepared by the contra-diffusion method do not demonstrate comparable ion separation capability (Li^+/Mg^{2+} selectivity <5) as well (Figure S7). The UiO-66 and UiO-66-NH_2 particles show positive charge in water,[39] which is not favorable for conducting cations. Although UiO-66-SO_3H possesses a negative charge for driving cation transport, its growth in PET nanochannels is challenging, which brings empty voids and defects that deteriorate the ion selectivity.

Concentration-Dependent Ion Transport Property. The ion conductance for monovalent cations increases significantly with the increasing ion concentration, while that of divalent cations is maintained at low levels (Figure 2C). Figure 2D exhibits a similar increasing trend of ion selectivity with the increase of ion concentrations from 10^{-3} to 10^{-1} M. At the highest ion salinity (e.g., 1 M), although a decrease of

https://doi.org/10.1021/jacs.4c02477
J. Am. Chem. Soc. 2024, 146, 14058−14066

ion selectivity appears, the selectivities of K^+/Mg^{2+}, Na^+/Mg^{2+}, and Li^+/Mg^{2+} are maintained at 1348, 857, and 325, respectively, which are encouraging outcomes for practical high-salinity ion separations. When the ions passing through MOF pores are at low concentrations, the conduction of monovalent ions and the binding of divalent ions are both achievable. With the increase of ion numbers inside of MOFs, ion binding sites become saturated, allowing more divalent cations to transport through the MOF channels (as shown in the increasing ion current values in Figure S8), resulting in a drop in ion selectivity.

pH-Dependent Ion Transport Property. The charging states of MOF particles are pH-dependent, showing an increasing negative charge from pH 2 to 8 (Figure 3A). Figure 3B shows that ion selectivity could be tuned over this pH range, with neutral to basic conditions favoring higher ion selectivity (up to 4042 for K^+/Mg^{2+}, 2556 for Na^+/Mg^{2+}, and 1199 for Li^+/Mg^{2+} at pH 8.0) compared to acidic conditions. Corresponding $I-V$ curves are shown in Figure S9, which exhibited that the ion current values at +1 V increase with the rise of pH from 6.0 to 8.0. Therefore, the increase in ion selectivity at higher pH results from the enhanced surface charge density and ion conductance capability of the membrane. The UiO-66-$(SH)_2$ membrane also demonstrates proton ion (H^+) conductance when pH drops to 2.0, as shown from the same ion current values at +1 V (Figure S9A). As pH 2.0 is close to the isoelectric point of the −SH groups in MOF particles (Figure 3A), the conductance for H^+ may be attributed to weak hydrogen bonds[40,41] formed by thiol groups in the membrane. The PXRD patterns of MOF particles treated with different pH of solutions were also conducted, indicating good stability of the materials from pH 2.0 to 8.0 (Figure S10).

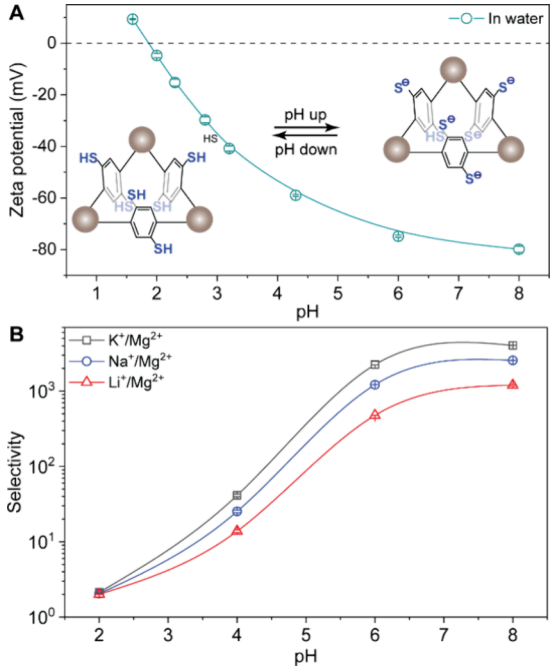

Figure 3. Zeta potentials of UiO-66-$(SH)_2$ particles in water of different pH values (A) and ion selectivity changes as a function of solution pH (B).

MD Simulations on Selective Ion Transport. MD simulations were performed to investigate the energy barrier of ions, one critical factor determining ion sieving performance within MOF channels.[42] The potential of mean force (PMF) profiles was calculated for K^+, Li^+, and Mg^{2+} ions migrating along the [111] direction, which connects the small [S] and large [L] cavities by crossing the MOF windows [W] for the MD simulation system (Figure 4A, Figure S11, and Tables S4 and S5 in Supporting Information). Figure 4B shows that the highest energy barrier for Mg^{2+} passing through the window [W] was significantly higher (68.8 kJ mol^{-1}) compared to those for K^+ (9.2 kJ mol^{-1}) or Li^+ (10.2 kJ mol^{-1}). K^+ encounters a lower energy barrier near the small cavity [S], while Li^+ experiences a lower energy barrier at the location of [W]. The energy barrier for Mg^{2+} is higher in regions between [W] and [S] but starts to drop when Mg^{2+} migrates toward the large cavity [L]. Therefore, different cations exhibit varied preferences for stay locations: K^+ chooses [S], Li^+ favors [W], and Mg^{2+} prefers [L]. The energy profiles are influenced by the dehydration processes of metal ions and specific ion−MOF interactions in the nano- and subnano-confined spaces.

The radial distribution functions (RDFs) between cations and sulfur at different locations, shown as $g(r)^{ion\text{-}S}$, are illustrated in Figure 4C to reveal the microstructural arrangement[43] of −SH groups around metal ions. The values of the x-axis and y-axis evaluate the probability of finding an S atom at a distance r around a metal ion located at the three specific locations: [L], [W], and [S]. For Mg^{2+} ions, they exhibit closer proximity and more pronounced distribution of S atoms when they stay at location [L], compared with those at locations [W] and [S]. Li^+ is closer to S in the location of [W], and the S distribution around Li^+ is similar at [L] and [W], which is slightly higher than at [S]. The proximity of S atoms to K^+ ions at locations [W] and [L] becomes closer than that at location [S]. However, the distribution of S atoms around them is lower compared to those of Mg^{2+} and Li^+ ions at [W] and [L] locations. The RDF results reveal the difference in ion-S distance and S distributions when ions move freely within MOF channels. Mg^{2+} displays a distinct increase in S atom distributions during migration from small to large cavities, exhibiting the most pronounced S distributions at location [L]. This aligns with their most preferred positioning in the larger cavity, consistent with experimental evidence of a higher binding interaction between Mg^{2+} and thiol groups.

The hydration number of water molecules surrounding the cations was further compared to find out the dehydration difference[37] of K^+, Li^+, and Mg^{2+} ions in MOF channels (Figure 4D). When K^+ ions migrate from the large cavity to the small cavity via the window, some water molecules in the first hydration shell are displaced (from ∼8 to ∼5) to the second hydration shell (from ∼3 to ∼6), with −SH groups occupying their previous positions. This can be observed in Figure 4C, showing −SH groups getting closer to K^+ ions at locations [W] and [L], and in Figure S12, where −SH directly contacts K^+ ions at those locations. The rearrangements correspond to the slight increase in energy barriers for K^+ ions migrating from small to large cavities. For both Li^+ and Mg^{2+}, however, their first hydration shells remain intact throughout the migration (the hydration number is 4 for Li^+ and 6 for Mg^{2+}). For the second hydration shell, Mg^{2+} experiences dehydration (the hydration number changes from ∼10 to ∼8) when migrating from [L] to [S], which aligns with the increase of energy barriers when they migrate from large to small cavity, while the change in the second hydration number for Li^+ is small, slightly fluctuating between ∼5 and ∼6.5. Simulated

https://doi.org/10.1021/jacs.4c02477
J. Am. Chem. Soc. 2024, 146, 14058−14066

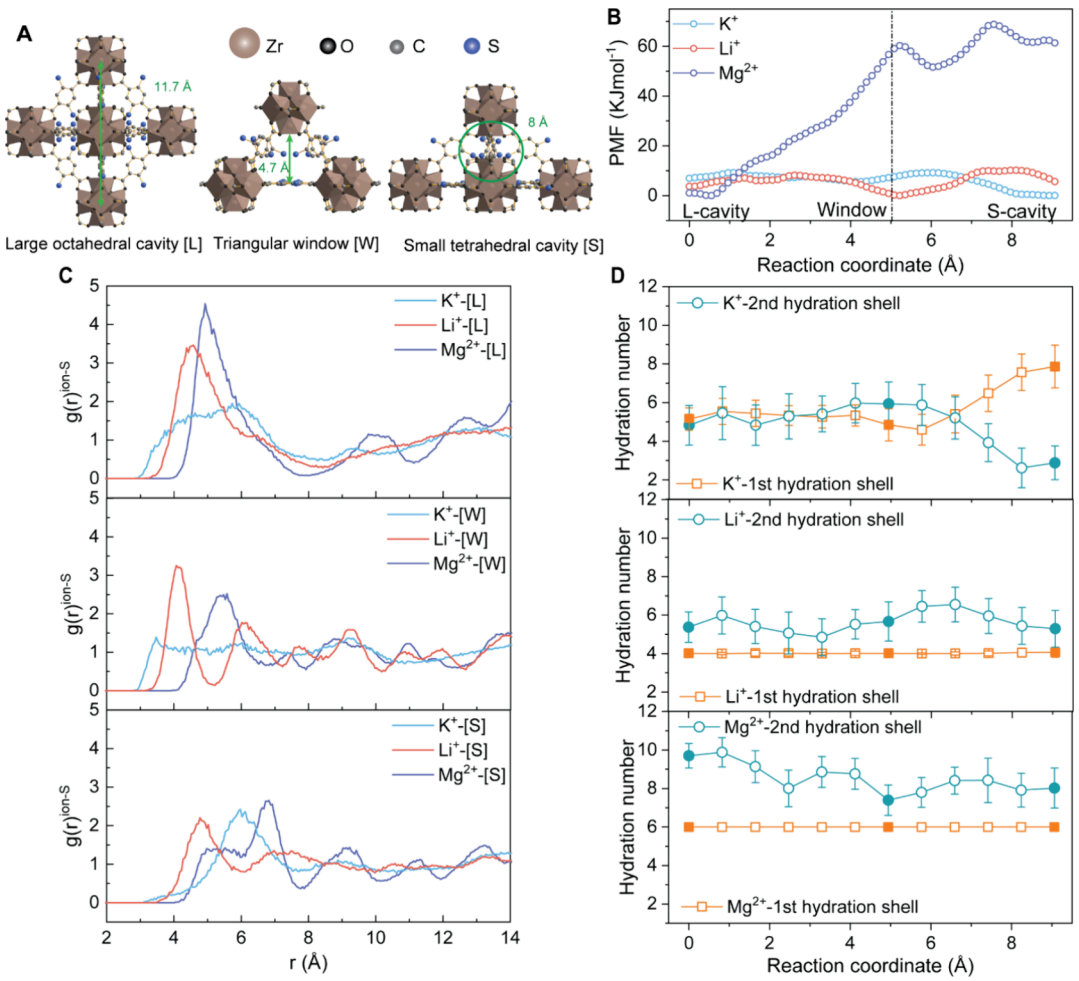

Figure 4. MD simulations on metal ion transport in UiO-66-$(SH)_2$ frameworks. (A) Schematics of the UiO-66-$(SH)_2$ MOF cell unit with different locations for ion transport in the large cavity [L], triangular window [W], and small cavity [S]. (B) Energy barriers for K^+, Li^+, and Mg^{2+} as a function of the distance to the large cavity center. (C) RDFs for ion density profiles as a function of the distance to sulfur atoms at the locations of [L], [W], and [S]. (D) Hydration numbers of water molecules for K^+, Li^+, and Mg^{2+} ions as a function of the distance from the large cavity center. The points shown in solid color represent locations of [L], [W], and [S], respectively.

images in Figure S12 depict ions after partial dehydration at different locations, including the ions in the center, the surrounding water molecules from two hydration shells, and the ligands with −SH groups. These results indicate that a strong binding interaction between Mg^{2+} and −SH groups of MOFs and associated dehydration effects are critical in realizing high K^+/Mg^{2+} and Li^+/Mg^{2+} selectivity.

Separation of Li^+ from Mixed Salt Solutions. The ion separation performance of the UiO-66-$(SH)_2$ membrane is based on the *I*−*V* measurement of single salt solutions. To further investigate its performance in mixed-ion separation, dual mixed-ion diffusion was performed under a constant electric field (+1 V). The membrane separation setup is shown in Figure 5A, consisting of a feed side with ion mixtures and a permeate side with water only. The concentration of diffused ions through the UiO-66-$(SH)_2$ membrane is time-dependent. In a preliminary separation experiment with equal concentrations of K^+ and Mg^{2+} (mole ratio of 1:1) within 96 h (Figure 5B), the concentration of K^+ kept increasing with time while the Mg^{2+} concentration gradually decreased, which means that the membrane can maintain the ion sieving capability over this period.

Different monovalent cations with Mg^{2+} at the same concentration were first separated within 96 h, and the selectivity performance is shown in Figure 5C. In the permeate, the separation of K^+ from Mg^{2+} is the most significant, with the highest selectivities reaching 2.3×10^3, followed by Na^+/Mg^{2+} and Li^+/Mg^{2+} whose highest selectivities were 3.9×10^2 and 1.8×10^2, respectively. These ion selectivity levels exhibited by dual-ion diffusion are consistent with the *I*−*V* measurement by pure salts.

To further evaluate the Li^+/Mg^{2+} separation capability of the UiO-66-$(SH)_2$ membrane toward salt-lake brines, the feed side solution was varied by changing the Mg^{2+}/Li^+ mole ratio from low to high, gradually close to the components of brines. As exhibited in Figure 5D, the Li^+/Mg^{2+} separation achieves a high performance up to ∼1516 when the Mg^{2+}/Li^+ ratio is at the lowest (0.2:1). With the rise of the Mg^{2+} concentration, the Li^+/Mg^{2+} selectivity declines to ∼185 at equal concentrations (1:1) and then drops to ∼70 at the ratio of 14:1 and ∼19 at the highest concentration (30:1). It is worth noting that the first two feed solutions contained relatively low concentrations of Mg^{2+}, less than 1 M, while the last two feed solutions contained very high salinity of Mg^{2+}, reaching 3−3.5 M, which is rarely investigated. Moreover, with the rise of the Mg^{2+}

https://doi.org/10.1021/jacs.4c02477
J. Am. Chem. Soc. 2024, 146, 14058−14066

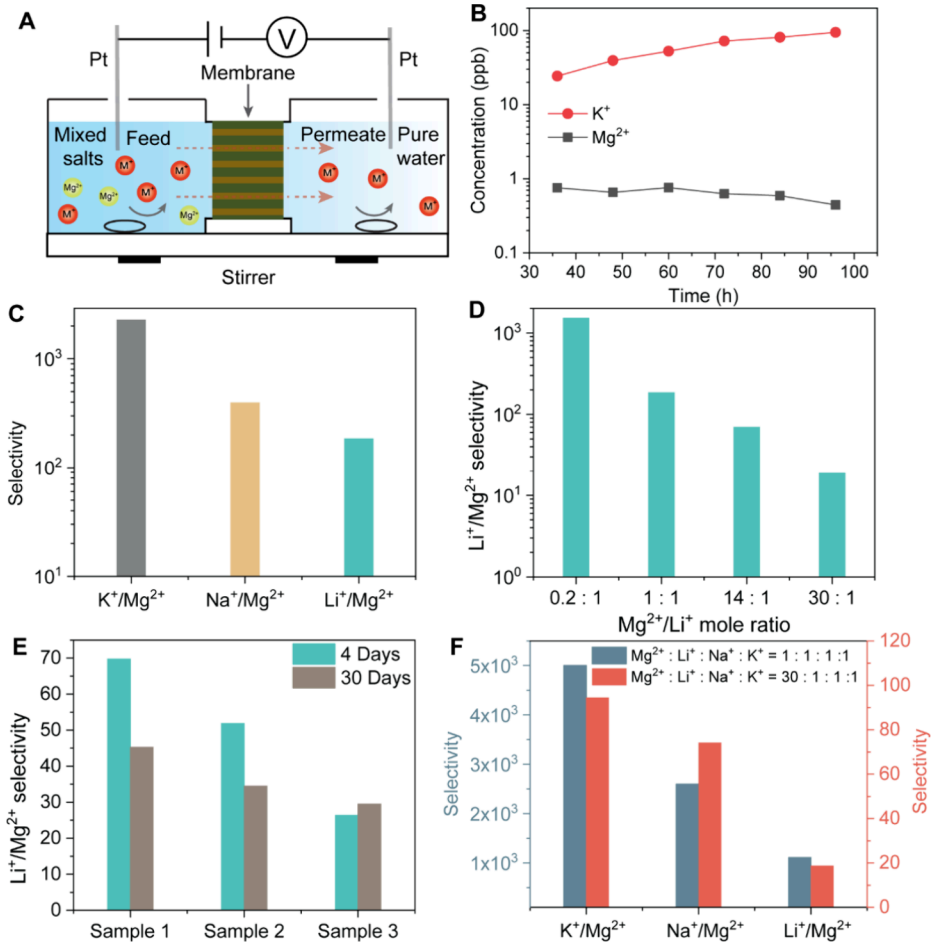

Figure 5. Ion separation performance at mixed-ion conditions. (A) Schematic illustration of membrane separation device for mixed-ion diffusion. (B) Ion concentration changes in the permeate side as a function of diffusion time. (C) Separation of different monovalent cations against Mg^{2+} with the same M^+/Mg^{2+} mole ratio (1:1). (D) Separation of Li^+ with different Mg^{2+}/Li^+ mole ratios. (E) Separation of Li^+ with a fixed Mg^{2+}/Li^+ mole ratio (14:1) in short and long periods. (F) Ion selectivity performance for simulated brine solutions containing multi-ions at low and high Mg^{2+}/M^+ mole ratios.

concentrations from 0.2 to 3.5 M, the permeation rate of Li^+ reduces from ~11.8 to ~0.6 mol m^{-2} h^{-1} and that of Mg^{2+} does not increase very significantly (Figure S13).

To ensure the long-term separation performance, the Li^+/Mg^{2+} separation was further investigated as a function of diffusion time, with the feed side filled with Mg^{2+}/Li^+ solutions at a relatively high mole ratio (14:1) and a high Mg^{2+} concentration of 3.5 M. Three replicates of membranes were used for the diffusion. Encouragingly, the Li^+/Mg^{2+} selectivity ranges between ~26 and ~70 within 4 days and are maintained between ~29 and ~45 when the diffusion period extended to 30 days (Figure 5E).

To further evaluate the membrane's ion separation performance against real brines containing multiple ions, four-cation (K^+, Na^+, Li^+, and Mg^{2+}) salt mixtures with low (1:1) and high (30:1) Mg^{2+}/M^+ mole ratios were utilized as the feed solutions for the practical lithium extraction study. As shown in Figure 5F, the K^+/Mg^{2+} selectivity is the highest with a value of 5004 and the selectivities for Na^+/Mg^{2+} and Li^+/Mg^{2+} in the permeate are also significantly increased to 2599 and 1114, respectively, in the Mg^{2+}/M^+ of 1:1 mixed condition, one order of magnitude higher than that of the dual-ion system. Faster transport of K^+ in the ion mixture seems to be beneficial for decreasing the diffusion of Mg^{2+}, which increases the overall ion selectivity and differs from the conventional understanding that membrane selectivity is normally decreased in multiple-component separation. Furthermore, the Li^+/Mg^{2+} selectivity in the Mg^{2+}/M^+ of 30:1 mixed condition is 19, which is equal to that of the dual-ion system, confirming the Li^+/Mg^{2+} separation capability of the UiO-66-$(SH)_2$ membrane for real lithium separation in harsh conditions. Compared with reported MOF membranes, the UiO-66-$(SH)_2$ membranes exhibit competitive lithium separation performance, especially for treating both equal and high Mg^{2+}/Li^+ mole ratio synthetic brines (Figure S14 and Table S6). Furthermore, the ion selectivity of the membrane can be repeated by multiple tests (Figure S15) and the MOF powders demonstrate almost unchanged PXRD patterns after soaking in tested salt solutions, including highly concentrated solutions tested up to 1 week (Figure S16), showing the stability of the MOFCMs and the MOF material UiO-66-$(SH)_2$.

CONCLUSIONS

Thiol-functionalized MOFCMs with impressive ion rectification and outstanding monovalent/divalent ion selectivity have been successfully developed, showing great promise for Li^+/Mg^{2+} separation. The experimental characterizations and theoretical simulations have revealed that the ion−sulfur

https://doi.org/10.1021/jacs.4c02477
J. Am. Chem. Soc. 2024, 146, 14058−14066

interactions and ion-dehydration dynamics through the thiolated MOF channels collectively influence the overall energy barriers determining ion sieving performance. The developed membranes can selectively conduct Li^+ over Mg^{2+} and sustainably extract limited Li^+ from sufficient Mg^{2+} synthetic brines with efficiencies between 10^1 and 10^3 in dual-ion systems and multi-ion systems. This work demonstrates that shaping current MOFCMs with versatile functional groups toward excellent ion binding/blockage capability is an efficient strategy to radically boost the Li^+/Mg^{2+} separation performance for real industry applications. These findings provide a new way to develop various MOFCMs decorated by different types of "ion binders" or the opposite "ion-conductors" to render challenging tasks of precise extractions of valuable ions.

■ ASSOCIATED CONTENT

Supporting Information

The Supporting Information is available free of charge at https://pubs.acs.org/doi/10.1021/jacs.4c02477.

Experimental methods for MOF membrane fabrication, characterization of MOF and MOF membranes, ion current measurement, mixed-ion diffusion measurement, ion selectivity calculation, ion permeation rate calculation, MD simulations, and supporting figures and tables (PDF)

■ AUTHOR INFORMATION

Corresponding Authors

Jue Hou − *Chemical and Environmental Engineering, School of Engineering, RMIT University, Melbourne, Victoria 3000, Australia;* orcid.org/0000-0003-0325-6979; Email: jue.hou@rmit.edu.au

Jefferson Zhe Liu − *Department of Mechanical Engineering, The University of Melbourne, Parkville, VIC 3010, Australia;* orcid.org/0000-0002-5282-7945; Email: zhe.liu@unimelb.edu.au

Huacheng Zhang − *Chemical and Environmental Engineering, School of Engineering, RMIT University, Melbourne, Victoria 3000, Australia;* orcid.org/0000-0001-5464-2947; Email: huacheng.zhang@rmit.edu.au

Authors

Chen Zhao − *Chemical and Environmental Engineering, School of Engineering, RMIT University, Melbourne, Victoria 3000, Australia*

Fan Feng − *Department of Mechanical Engineering, The University of Melbourne, Parkville, VIC 3010, Australia*

Jian Hu − *Chemical and Environmental Engineering, School of Engineering, RMIT University, Melbourne, Victoria 3000, Australia*

Yuyu Su − *Chemical and Environmental Engineering, School of Engineering, RMIT University, Melbourne, Victoria 3000, Australia;* orcid.org/0009-0000-4008-3005

Matthew Hill − *Department of Chemical and Biological Engineering, Monash University, Clayton, Victoria 3800, Australia;* orcid.org/0000-0001-8897-0324

Benny D. Freeman − *Department of Chemical and Biological Engineering, Monash University, Clayton, Victoria 3800, Australia;* orcid.org/0000-0003-2779-7788

Huanting Wang − *Department of Chemical and Biological Engineering, Monash University, Clayton, Victoria 3800, Australia;* orcid.org/0000-0002-9887-5555

Complete contact information is available at: https://pubs.acs.org/10.1021/jacs.4c02477

Author Contributions

#C.Z. and F.F. contributed equally to this paper.

Author Contributions

All authors have given approval to the final version of the manuscript.

Notes

The authors declare no competing financial interest.

■ ACKNOWLEDGMENTS

This work was supported by the Australian Research Council (FT200100259, DE220100435, and DP210103888). The authors acknowledge the great help from Dr Kim Chung Nguyen, Dr Qi Han, and Dr Paramita Koley from RMIT University and Dr Anthony De Girolamo from Monash University. The authors acknowledge the facilities, and the scientific and technical assistance of the RMIT University's Microscopy & Microanalysis Facility, a linked laboratory of the Microscopy Australia, enabled by NCRIS. This work was performed in part at the RMIT Micro Nano Research Facility (MNRF) in the Victorian Node of the Australian National Fabrication Facility (ANFF). The employed PET films are part of a UMAT experiment, which was performed at the beamline X0 at the GSI Helmholtzzentrum für Schwerionenforschung, Darmstadt (Germany), in the frame of FAIR-Phase 0.

■ REFERENCES

(1) Razmjou, A.; Asadnia, M.; Hosseini, E.; Korayem, A. H.; Chen, V. Design Principles of Ion Selective Nanostructured Membranes for the Extraction of Lithium Ions. *Nat. Commun.* **2019**, *10* (1), 5793.

(2) Wang, W.; Zhang, Y.; Tan, M.; Xue, C.; Zhou, W.; Bao, H.; Hon Lau, C.; Yang, X.; Ma, J.; Shao, L. Recent Advances in Monovalent Ion Selective Membranes Towards Environmental Remediation and Energy Harvesting. *Sep. Purif. Technol.* **2022**, *297*, No. 121520.

(3) Xu, T.; Wu, B.; Hou, L.; Zhu, Y.; Sheng, F.; Zhao, Z.; Dong, Y.; Liu, J.; Ye, B.; Li, X.; Ge, L.; Wang, H.; Xu, T. Highly Ion-Permselective Porous Organic Cage Membranes with Hierarchical Channels. *J. Am. Chem. Soc.* **2022**, *144* (23), 10220−10229.

(4) Lu, Z.; Wu, Y.; Ding, L.; Wei, Y.; Wang, H. A Lamellar Mxene (Ti_3C_2Tx)/Pss Composite Membrane for Fast and Selective Lithium-Ion Separation. *Angew. Chem., Int. Ed.* **2021**, *60* (41), 22265−22269.

(5) Razmjou, A.; Eshaghi, G.; Orooji, Y.; Hosseini, E.; Korayem, A. H.; Mohagheghian, F.; Boroumand, Y.; Noorbakhsh, A.; Asadnia, M.; Chen, V. Lithium Ion-Selective Membrane with 2D Subnanometer Channels. *Water Res.* **2019**, *159*, 313−323.

(6) Ruan, X.; Zhang, C.; Zhu, Y.; Cai, F.; Yang, Y.; Feng, J.; Ma, X.; Zheng, Y.; Li, H.; Yuan, Y.; Zhu, G. Constructing Mechanical Shuttles in a Three-Dimensional (3D) Porous Architecture for Selective Transport of Lithium Ions. *Angew. Chem., Int. Ed.* **2023**, *62* (7), No. e202216549.

(7) Wen, Q.; Yan, D.; Liu, F.; Wang, M.; Ling, Y.; Wang, P.; Kluth, P.; Schauries, D.; Trautmann, C.; Apel, P.; Guo, W.; Xiao, G.; Liu, J.; Xue, J.; Wang, Y. Highly Selective Ionic Transport through Subnanometer Pores in Polymer Films. *Adv. Funct. Mater.* **2016**, *26* (32), 5796−5803.

(8) Zhu, B.; Shao, R.; Li, N.; Guo, C.; Liu, P.; Shi, J.; Min, C.; Liu, S.; Qian, X.; Wang, L.; Xu, Z. Narrowing the Pore Size Distribution of Polyamide Nanofiltration Membranes Via Dragging Piperazines to Enhance Ion Selectivity. *J. Membr. Sci.* **2023**, *667*, No. 121187.

(9) Zhang, H.; Li, X.; Hou, J.; Jiang, L.; Wang, H. Angstrom-Scale Ion Channels Towards Single-Ion Selectivity. *Chem. Soc. Rev.* **2022**, *51* (6), 2224−2254.
(10) Li, X.; Zhang, H.; Hou, J.; Ou, R.; Zhu, Y.; Zhao, C.; Qian, T.; Easton, C. D.; Selomulya, C.; Hill, M. R.; Wang, H. Sulfonated Sub-1-nm Metal-Organic Framework Channels with Ultrahigh Proton Selectivity. *J. Am. Chem. Soc.* **2020**, *142* (21), 9827−9833.
(11) Hou, J.; Zhang, H.; Thornton, A. W.; Hill, A. J.; Wang, H.; Konstas, K. Lithium Extraction by Emerging Metal-Organic Framework-Based Membranes. *Adv. Funct. Mater.* **2021**, *31* (46), No. 2105991.
(12) Li, X.; Hill, M. R.; Wang, H.; Zhang, H. Metal-Organic Framework-Based Ion-Selective Membranes. *Adv. Mater. Technol.* **2021**, *6* (10), No. 2000790.
(13) Qiu, M.; Zhu, Z.; Wang, D.; Xu, Z.; Miao, W.; Jiang, L.; Tian, Y. Large-Scale Metal-Organic Framework Nanoparticle Monolayers with Controlled Orientation for Selective Transport of Rare-Earth Elements. *J. Am. Chem. Soc.* **2023**, *145* (22), 12275−12283.
(14) Zhao, C.; Hou, J.; Hill, M.; Freeman, B.; Wang, H.; Zhang, H. Enhanced Gating Effects in Responsive Sub-Nanofluidic Ion Channels. *Acc. Mater. Res.* **2023**, *4* (9), 786−797.
(15) Liu, X.; Demir, N. K.; Wu, Z.; Li, K. Highly Water-Stable Zirconium Metal-Organic Framework UiO-66 Membranes Supported on Alumina Hollow Fibers for Desalination. *J. Am. Chem. Soc.* **2015**, *137* (22), 6999−7002.
(16) Xie, S.; Monnens, W.; Zhang, W.; Guo, W.; Han, N.; Zhou, Z.; Xue, Z.; Vankelecom, I. F. J.; Zhang, X.; Fransaer, J. Control over Cathodic Deposition of Continuous UiO-66 Films for Ion-Selective Transport. *Cell Rep. Phys. Sci.* **2023**, *4* (5), No. 101412.
(17) Xu, T.; Shehzad, M. A.; Yu, D.; Li, Q.; Wu, B.; Ren, X.; Ge, L.; Xu, T. Highly Cation Permselective Metal-Organic Framework Membranes with Leaf-Like Morphology. *ChemSusChem* **2019**, *12* (12), 2593−2597.
(18) Xiao, H.; Chai, M.; Hosseini, A.; Korayem, A. H.; Abdollahzadeh, M.; Ahmadi, H.; Chen, V.; Gore, D. B.; Asadnia, M.; Razmjou, A. UiO-66-$(COONa)_2$ Membrane with Programmable Ionic Channels for Lithium Ion-Selective Transport. *J. Membr. Sci.* **2023**, *670*, No. 121312.
(19) Xiao, H.; Chai, M.; Abdollahzadeh, M.; Ahmadi, H.; Chen, V.; Gore, D. B.; Asadnia, M.; Razmjou, A. A Lithium Ion Selective Membrane Synthesized from a Double Layered Zrbased Metalorganic Framework (Mof-on-Mof) Thin Film. *Desalination* **2022**, *532*, No. 115733.
(20) Xu, R.; Kang, Y.; Zhang, W.; Zhang, X.; Pan, B. Oriented UiO-67 Metal-Organic Framework Membrane with Fast and Selective Lithium-Ion Transport. *Angew. Chem., Int. Ed.* **2022**, *61* (3), No. e202115443.
(21) Liang, H.; Guo, Y.; Peng, X.; Chen, B. Light-Gated Cation-Selective Transport in Metal-Organic Framework Membranes. *J. Mater. Chem. A* **2020**, *8* (22), 11399−11405.
(22) Guo, Y.; Ying, Y.; Mao, Y.; Peng, X.; Chen, B. Polystyrene Sulfonate Threaded through a Metal-Organic Framework Membrane for Fast and Selective Lithium-Ion Separation. *Angew. Chem., Int. Ed.* **2016**, *55* (48), 15120−15124.
(23) Li, J.; Shi, Y.; Qi, C.; Zhang, B.; Xing, X.; Li, Y.; Chen, T.; Mao, X.; Zuo, Z.; Zhao, X.; Pan, Z.; Li, L.; Yang, X.; Li, C. Charging Metal-Organic Framework Membranes by Incorporating Crown Ethers to Capture Cations for Ion Sieving. *Angew. Chem., Int. Ed.* **2023**, *62* (40), No. e202309918.
(24) Xu, T.; Sheng, F.; Wu, B.; Shehzad, M. A.; Yasmin, A.; Wang, X.; He, Y.; Ge, L.; Zheng, X.; Xu, T. Ti-Exchanged UiO-66-NH_2−Containing Polyamide Membranes with Remarkable Cation Permselectivity. *J. Membr. Sci.* **2020**, *615*, No. 118608.
(25) Zhang, C.; Mu, Y.; Zhang, W.; Zhao, S.; Wang, Y. Pvc-Based Hybrid Membranes Containing Metal-Organic Frameworks for Li^+/Mg^{2+} Separation. *J. Membr. Sci.* **2020**, *596*, No. 117724.
(26) Zeng, X.; Xu, L.; Deng, T.; Wang, Y.; Xu, W.; Zhang, W. Anionic Mofs Embedded in Anion-Exchange Membranes for the Separation of Lithium/Magnesium Cations. *ACS Sustain. Chem. Eng.* **2023**, *11* (35), 12877−12887.
(27) Tao, L.; Wang, X.; Wu, F.; Wang, B.; Gao, C.; Gao, X. Highly Efficient Li^+/Mg^{2+} Separation of Monovalent Cation Permselective Membrane Enhanced by 2D Metal Organic Framework Nanosheets. *Sep. Purif. Technol.* **2022**, *296*, No. 121309.
(28) Hou, J.; Zhang, H.; Lu, J.; Li, X.; Zhao, C.; Wang, H.; Thornton, A. W.; Konstas, K. Influence of Surface Chemistry and Channel Shapes on the Lithium-Ion Separation in Metal-Organic-Framework-Nanochannel Membranes. *J. Membr. Sci.* **2023**, *674*, No. 121511.
(29) Wu, Z.; Li, C.; Huang, C.; Cheng, S.; Ouyang, X.; Chen, W.; Zhang, P.; Jiang, Y.; Jiang, L. Wettability-Regulated Synthesis of Metal-Organic Framework Array with Subnanochannels Enables Efficient Separation of Mono-/Multivalent Metal Ions. *Chem.—Eur. J.* **2023**, *29* (39), No. e202301163.
(30) Sanjuan, B.; Gourcerol, B.; Millot, R.; Rettenmaier, D.; Jeandel, E.; Rombaut, A. Lithium-Rich Geothermal Brines in Europe: An up-Date About Geochemical Characteristics and Implications for Potential Li Resources. *Geothermics* **2022**, *101*, No. 102385.
(31) Zhang, T.; Zheng, W.; Wang, Q.; Wu, Z.; Wang, Z. Designed Strategies of Nanofiltration Technology for Mg^{2+}/Li^+ Separation from Salt-Lake Brine: A Comprehensive Review. *Desalination* **2023**, *546*, No. 116205.
(32) Leus, K.; Perez, J. P. H.; Folens, K.; Meledina, M.; Van Tendeloo, G.; Du Laing, G.; Van Der Voort, P. UiO-66-$(SH)_2$ as Stable, Selective and Regenerable Adsorbent for the Removal of Mercury from Water under Environmentally-Relevant Conditions. *Faraday Discuss.* **2017**, *201*, 145−161.
(33) Yee, K. K.; Reimer, N.; Liu, J.; Cheng, S. Y.; Yiu, S. M.; Weber, J.; Stock, N.; Xu, Z. Effective Mercury Sorption by Thiol-Laced Metal-Organic Frameworks: In Strong Acid and the Vapor Phase. *J. Am. Chem. Soc.* **2013**, *135* (21), 7795−7798.
(34) Apel, P. Y.; Blonskaya, I. V.; Dmitriev, S. N.; Orelovitch, O. L.; Presz, A.; Sartowska, B. A. Fabrication of Nanopores in Polymer Foils with Surfactant-Controlled Longitudinal Profiles. *Nanotechnol.* **2007**, *18* (30), No. 305302.
(35) Nightingale, E., Jr. Phenomenological Theory of Ion Solvation. Effective Radii of Hydrated Ions. *J. Phys. Chem.* **1959**, *63* (9), 1381−1387.
(36) Hou, J.; Zhang, H.; Wang, H.; Thornton, A. W.; Konstas, K. Amphoteric Metal-Organic Framework Subnanochannels with pH-Tuneable Cation and Anion Sieving Properties. *J. Mater. Chem. A* **2023**, *11*, 13223−13230.
(37) Lu, J.; Zhang, H.; Hou, J.; Li, X.; Hu, X.; Hu, Y.; Easton, C. D.; Li, Q.; Sun, C.; Thornton, A. W.; Hill, M. R.; Zhang, X.; Jiang, G.; Liu, J. Z.; Hill, A. J.; Freeman, B. D.; Jiang, L.; Wang, H. Efficient Metal Ion Sieving in Rectifying Subnanochannels Enabled by Metal-Organic Frameworks. *Nat. Mater.* **2020**, *19* (7), 767−774.
(38) Lu, J.; Zhang, H.; Hu, X.; Qian, B.; Hou, J.; Han, L.; Zhu, Y.; Sun, C.; Jiang, L.; Wang, H. Ultraselective Monovalent Metal Ion Conduction in a Three-Dimensional Sub-1 nm Nanofluidic Device Constructed by Metal-Organic Frameworks. *ACS Nano* **2021**, *15* (1), 1240−1249.
(39) Li, X.; Zhang, H.; Wang, P.; Hou, J.; Lu, J.; Easton, C. D.; Zhang, X.; Hill, M. R.; Thornton, A. W.; Liu, J. Z.; Freeman, B. D.; Hill, A. J.; Jiang, L.; Wang, H. Fast and Selective Fluoride Ion Conduction in Sub-1-Nanometer Metal-Organic Framework Channels. *Nat. Commun.* **2019**, *10* (1), 2490.
(40) Lobo, I. A.; Robertson, P. A.; Villani, L.; Wilson, D. J. D.; Robertson, E. G. Thiols as Hydrogen Bond Acceptors and Donors: Spectroscopy of 2-Phenylethanethiol Complexes. *J. Phys. Chem. A* **2018**, *122* (36), 7171−7180.
(41) Paul, A.; Thomas, R. Evidences for Sulfur Centered Hydrogen Bond with Sulfur Atoms as a Donor in Aromatic Thiols and Aliphatic Thiols in Aqueous Solution. *J. Mol. Liq.* **2022**, *348*, No. 118078.
(42) Abdollahzadeh, M.; Chai, M.; Hosseini, E.; Zakertabrizi, M.; Mohammad, M.; Ahmadi, H.; Hou, J.; Lim, S.; Korayem, A. H.; Chen, V.; Asadnia, M.; Razmjou, A. Designing Angstrom-Scale Asymmetric

Mof-on-Mof Cavities for High Monovalent Ion Selectivity. *Adv. Mater.* **2022**, *34* (9), No. 2107878.
(43) Li, X.; Jiang, G.; Jian, M.; Zhao, C.; Hou, J.; Thornton, A. W.; Zhang, X.; Liu, J. Z.; Freeman, B. D.; Wang, H.; Jiang, L.; Zhang, H. Construction of Angstrom-Scale Ion Channels with Versatile Pore Configurations and Sizes by Metal-Organic Frameworks. *Nat. Commun.* **2023**, *14* (1), 286.

https://doi.org/10.1021/jacs.4c02477
J. Am. Chem. Soc. 2024, 146, 14058−14066